Applied Catalysis B: Environmental 247 (2019) 173–181

Contents lists available at ScienceDirect

Applied Catalysis B: Environmental

journal homepage: www.elsevier.com/locate/apcatb

Iron and other metal species as *phase-composition controllers* influencing the photocatalytic activity of TiO_2 materials

Marcin Surówka, Marcin Kobielusz, Mateusz Trochowski, Marta Buchalska, Krzysztof Kruczała, Paweł Broś, Wojciech Macyk*

Faculty of Chemistry, Jagiellonian University, ul. Gronostajowa 2, 30-387, Kraków, Poland

ARTICLE INFO

Keywords:
Photocatalysis
Modified titanium dioxide
Synthesis of photocatalysts
Phase composition

ABSTRACT

The goal of the work is to verify which properties of TiO_2-based materials, influenced by small amounts of Fe, Co, Ga, Bi, W, Mo, V and Ni species used as modifiers, play the predominant role in changing the photoactivity of TiO_2. Two groups of materials were studied: TiO_2 synthesized in the presence of nanocrystalline metal oxide and dissolved metal ions (cations or oxyanions). Sols were calcined at 450, 600 or 900°C. Physicochemical properties of the materials were characterized by XRD, DRS, SEM, EPR, porosimetry and photocurrent measurements. The most detailed studies were focused on modifications by iron species. TiO_2 doping was achieved for both Fe^{3+} and Fe_2O_3 modifiers after calcination at temperatures equal to or higher than 450 and 900°C, respectively. Morphology of the materials (phase composition, specific surface area, *etc.*) were influenced by iron species even if they were not introduced into the crystal lattice of TiO_2. Comparison of activity of photocatalysts and elucidation of the role of various reactive oxygen species were based on photooxidation tests involving Azure B and terephthalic acid. In general, iron species improved photocatalytic activity, nevertheless, doping of the materials appeared detrimental. A particular improvement of the activity was achieved for composites with low iron contents (*ca.* 0.01%mol Fe:Ti). The studies revealed, that beside the widely discussed mechanisms (photo-Fenton processes, charge separation, photosensitization, *etc.*) iron species can indirectly influence the photocatalytic activity of TiO_2 acting as *phase-composition controllers* (PCC) during the synthesis of this oxide, which determine morphology of the resulting photocatalyst. To support this hypothesis, several sets of other TiO_2 materials were modified with Co, Ga, Bi, W, Mo, V and Ni species. We show, that the use of these modifiers in small amounts can influence indirectly the activity of photocatalysts regardless to the type of modifier. Therefore different photoactivity of the tested materials should be attributed to these modifier-induced structural and electronic changes of the photocatalysts rather than to any other function of dopants, including photosensitization, enhanced charge separation, catalytic activity, at which most of studies are focused.

1. Introduction

Extensive research shows that doping of titanium dioxide with metal ions or combining with metal oxides can influence photocatalytic properties of the final material. For instance, the decrease of electron-hole recombination rate was proven for such photocatalysts [1–7]. The lifetime of photogenerated charges in the case of modified TiO_2 is often increased compared to the bare material, making phoitoinduced surface redox processes more efficient. In many cases such modifications may also result in TiO_2 photosensitization [8–10]. Furthermore, deposited metal oxides act as co-catalysts improving the overall photocatalytic efficiency [11]. Photocatalytic activity of modified TiO_2 was tested in several reactions, including photodegradation of dyes (*e.g.*, methylene blue [12–15], Acid red [16], rhodamine B [17]), arenes (*e.g.*, xylenes [2,18], toluene [2]), phenols (nitrophenols [19], chlorophenols [20]) and bacteria inactivation [21].

The mechanism of a photocatalytic reaction differs for various photocatalysts and depends on the properties of the modifier. Introduction of metal ions into TiO_2 crystals may generate new electron acceptor levels below the conduction band (CB) of titania (Fig. 1a). Similarly, in composite materials the modifier can play the role of the electron acceptor (Fig. 1b). The energy of generated charges and the direction of photoinduced charge transfer depend on the electronic (redox) properties of the modifier [22]. Formation of a heterojunction between, *e.g.*, *p*-NiO and *n*-TiO_2 leads to another type of the charge transfer mechanism. Photoexcited electrons can flow from NiO to the

* Corresponding author.
E-mail address: macyk@chemia.uj.edu.pl (W. Macyk).

https://doi.org/10.1016/j.apcatb.2019.01.074
Received 2 December 2018; Received in revised form 21 January 2019; Accepted 27 January 2019
Available online 29 January 2019

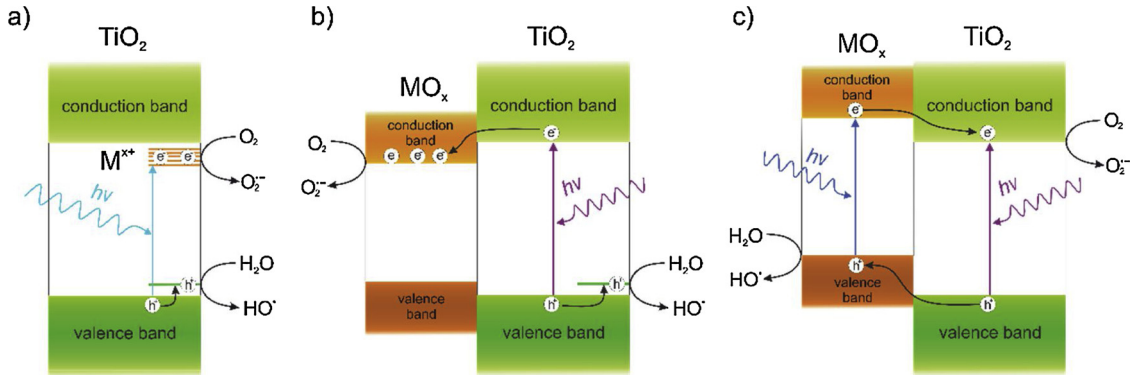

Fig. 1. Possible mechanisms of hydroxyl radicals and superoxide photogeneration in the M^{x+}/TiO_2 (a) and MO_x/TiO_2 (b, c) systems [23].

conduction band of TiO_2, while the hole injection from TiO_2 to the valence band of NiO can occur simultaneously (Fig. 1c) [22].

Iron ions and iron oxides are perhaps the most commonly studied and interesting dopants and modifiers of titanium(IV) oxide [24,25]. Doping with iron(III) species generates new electronic states below the conduction band (Fig. 1a). Electrons can be photoexcited from the valence band (VB) of TiO_2 directly to Fe^{III} states, which in some cases can act as oxygen reducing sites [26–30]. The increased charge separation was observed for some materials doped with W(VI) [16,31,32], Mo species [4,31], Ni(II) [2], Co(II) [33], Bi species [17] or V ions [5,15]. For many other materials a better charge separation, longer lifetime of photogenerated charges, increased concentration of oxygen vacancies [4] and better generation of reactive oxygen species [16] was confirmed.

Also other effects can be observed for various materials. It was proven that in small concentrations Ni(II) dopant acts as an electron trap. When its concentration is too high, Ni(II) becomes the recombination center which quenches photogenerated holes [34]. Molecular oxygen binds better to the surface of iron(III) oxide in the modified material so the rate of superoxide radicals generation can be higher than for non-modified TiO_2 [1]. Bismuth-doped titania nanotubes showed a higher specific surface area and surface hydroxyl groups concentration compared to undoped TiO_2 nanotubes. Bismuth was found to have the opposite effect on TiO_2 nanoparticles [17].

Titanium dioxide is often synthesized in the process of hydrolysis of titanium halides or alcoholates [35,36]. Calcination after hydrolysis leads to the formation of anatase and rutile phases, the ratio of which depends on applied parameters, including temperature and time [37]. Modifiers can influence the temperature and kinetics of anatase to rutile transformation [38]. For instance, synthesis of TiO_2 materials in the presence of cobalt ions hinders anatase to rutile transformation. The temperature of phase transition is higher than for unmodified materials [33,39]. Cobalt dopant also inhibits the growth of the composite crystals [39]. The crystal size can either decrease (for WO_3 [16,40]) or increase (for vanadium ions [15]) with the increasing concentration of dopants. It was also shown that in many cases doping with transition metal ions causes the decrease of the specific surface area of the final material [2].

Aforementioned desirable properties of the modified materials depend on the synthesis conditions. The optimal amount of the dopant, which is usually in the range of up to 3%wt (as reported in many papers [14–16,20,41]), can increase the activity of the material. Too high concentration of the modifier may distort the crystallinity of the composite and reduce its activity [2].

Modifiers can cause broadening of the light absorption by the photocatalyst. This effect was observed, *inter alia*, for TiO_2 materials doped with Fe [26,28,42,43], Co [44], Mo [4,44], V [15,44] and Ni [44]. The absorption edge of these materials is shifted up to 500 nm [44,45]. For cobalt-doped material also a separate band at 600 nm could be observed [44,45]. Absorption of visible light can also be achieved for composites of metal oxides with titania. For instance, this effect was observed for WO_3/TiO_2, but only in the case of non-calcined samples [16] or those calcined at low temperatures [3]. Similar properties were also observed for Fe_2O_3/TiO_2 composites [46]. It should be noted, that the absorption of visible light is a necessary, but not sufficient, condition for visible light induced photocatalytic activity of TiO_2-based materials.

Other processes can also be responsible for the increased activity of titanium dioxide modified with some transition metal admixtures, for instance Fenton, Fenton-like and photo-Fenton reactions [47,48]. Hydrogen peroxide, which is involved in these processes, can be generated at the surface of TiO_2 as a result of photocatalytic reduction of oxygen. Fenton reactions require specific conditions, including an appropriate pH, redox species (for instance the Fe^{II}/Fe^{III} couple) and the presence of H_2O_2. The concentration of hydrogen peroxide that is generated at the surface of TiO_2 is not high enough to induce a significant effect associated with the Fenton process for materials modified with Fe species. However, a high efficiency of the photo-Fenton process can be achieved by adding H_2O_2 to the system. The effect was recently reported for materials such as Fe/TiO_2 [49], α-Fe_2O_3/graphene system [50] and Fe-doped TiO_2/reduced graphene oxide [51].

This paper is aimed at verifying which properties of TiO_2-based materials, influenced by small amounts (0.01–0.50%mol, *i.e.* ~0.01–1.50%wt) of modifiers, used both as ionic dopants and oxides, play the predominant role in changing the photoactivity of these materials. Herein we present a detailed discussion based on the studies of TiO_2 materials modified with Fe, Co, Ga, Bi, W, Mo, V and Ni species.

2. Experimental section

2.1. Synthesis and characterisation of the materials

Materials based on titanium dioxide were synthesized by the sol-gel method. Titanium(IV) isopropoxide was used as the TiO_2 precursor. The solutions of salts ($Fe(NO_3)_3$; $Co(NO_3)_2$; $Ga(NO_3)_3$; $Bi(NO_3)_3$; Na_2WO_4; Na_2MoO_4; $NaVO_3$; $Ni(NO_3)_2$) and suspensions of oxides (Fe_2O_3; CoO; Ga_2O_3; Bi_2O_3; WO_3; MoO_3; V_2O_5; NiO) (*ca.* 20 cm^3) were prepared in water. The amounts of modifiers in the mixtures were adjusted to reach 0.01, 0.05, 0.25 or 0.50% M:Ti molar ratio in the final material. The solution of Ti(*i*-OPr)$_4$ (11.205 cm^3 in *ca.* 20 cm^3 of isopropanol) was added dropwise to the beaker with the modifier while stirring. The final suspension was stirred intensively for an hour. Solid materials were dried at 60°C, ground to powder and calcined at 450, 600 and 900°C for 4 h.

Diffuse reflectance spectra were collected in the range of 250–800 nm using a UV–vis spectrophotometer (*Shimadzu* UV-3600) equipped with a 15 cm diameter integrating sphere. Samples were ground with the reference material (1:300 by mass). Obtained spectra

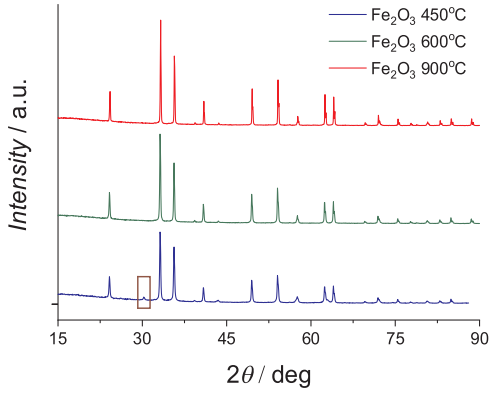

Fig. 2. Diffractograms of Fe_2O_3 calcined at different temperatures. The (206) facet of γ-Fe_2O_3 [34] is indicated in the frame.

were subsequently transformed to the Kubelka-Munk function.

The X-ray diffraction patterns were recorded using a *Rigaku* MiniFlex 600 diffractometer. The nanocrystalline powders were pressed inside the sample holder and the X-ray diffraction data were collected in the step scan mode. Cu K*α* was the X-ray radiation source operating at 40 kV, 15 mA. The scanning rate was 3 deg min^{-1} at a step of 0.05° in the 2*θ* range of 10-90°. Subsequently, integrals of reflexes at $2\theta = 25.3°$ and 27.3° (the most intensive reflexes for anatase and rutile, respectively) in recorded diffraction patterns were calculated. The measured peak areas were used to evaluate the content of titania crystal phases in the studied materials in comparison to reference samples of pure anatase and rutile (Fig. S1). The estimated error of the phase content determination did not exceed 3%.

Nitrogen adsorption-desorption isotherms were measured at 77 K using a *Micromeritics* ASAP 2020 instrument. Specific surface areas were calculated using the Brunauer–Emmett–Teller method within the relative pressure of $p/p_0 = 0.05\text{-}0.15$. The total pore volumes were obtained from the volumes of nitrogen adsorbed at $p/p_0 = 0.97$.

Photoelectrochemical measurements were carried out using *Autolab* PGSTAT302 N potentiostat and XBO-150 xenon lamp with light stabilization equipped with a monochromator (*Instytut Fotonowy*). Measurements have been done in a three-electrode cell using platinum wire and Ag/AgCl as counter and reference electrodes, respectively. A thin layer of the material deposited on ITO foil (resistivity: 60 Ω sq^{-1}) was used as a working electrode. The electrodes were placed in a quartz cuvette filled with 0.1 M KNO_3 (≥99.0%, *Sigma-Aldrich*) solution (pH = 6.1) in pure water (Milli-Q water) as an electrolyte. The measurements have been done after saturation of the electrolyte with argon (oxygen free conditions). Irradiation was done within the wavelength range of 380–600 nm. Photocurrent generation was measured within the potential range of –0.2-1.0 V *vs.* Ag/AgCl.

EPR measurements were carried out at room temperature using the *Bruker* Elexsys E-500 spectrometer operating at X-band (9.8 GHz) and 100 kHz magnetic field modulation equipped with a super high sensitivity cavity ER 4122 SHQE. Spectra of the materials (0.50%mol Fe:Ti) were recorded at 2 mW microwave power, time constant of 81.92 ms, conversion time of 163.84 ms. The value of *g*-factor was calculated from the spectra, using Bruker Elexsys E-500 software.

2.2. Photocatalytic activity

The reaction of terephthalic acid (TA) to hydroxyterephthalic acid (TAOH) oxidation is one of the specific probes enabling comparison of efficiencies of hydroxyl radicals formation (SI, Fig. S6) [52]. The product of the reaction shows good fluorescence in contrast to the substrate. Thesuspensions of TiO_2-based materials (1 g dm^{-3}) in TA solution ($3{\cdot}10^{-3}$ M; pH = 8) were simultaneously aerated and irradiated with xenon lamp (XBO-150) through the cut-off filter $\lambda > 320$ nm and the filter made of the $CuSO_4$ solution (cutting on at *ca.* 700 nm). Formation of TAOH was monitored by collecting emission spectra ($\lambda_{ex} = 315$ nm; emission 320–600 nm; $\lambda_{max} = 426$ nm; *Perkin-Elmer* LS55). The results are presented as TAOH formation rates calculated from the linear regression fitted to collected data, assuming a pseudo-zeroth-order kinetics (more details in SI, Fig. S7).

The $2.5{\cdot}10^{-5}$ M ($A_{652} = 1.0$) solution of Azure B (AB) was irradiated in the presence of TiO_2 materials (1 g dm^{-3}) with the same setup as for TA photocatalytic tests, however, in this case a band-pass filter (325 nm < λ < 500 nm) was used instead of the cut-off filter. Degradation of AB was monitored by UV–vis absorbance measurements ($\lambda_{max} = 652$ nm). Rate constants were calculated assuming the first order kinetics.

3. Results and discussion

3.1. Characterization of iron(III)-modified materials

Non-modified materials and materials containing 0.01% of modifiers were white. The other powders were slightly orange, with the colour intensifying with the increasing content of Fe^{III} species. XRD patterns of bare Fe_2O_3 are very similar regardless of the calcination temperature. The material appeared to be α-Fe_2O_3 with a small admixture of the γ form when calcined at 450°C (Fig. 2). A small peak characteristic for (206) facet of γ-Fe_2O_3 could be observed [34].

Due to small concentrations of the modifiers in the studied materials, no peaks associated with iron(III) oxides were recorded (Fig. S2). Crystal phase composition of TiO_2 is shown in Fig. 3. Mean sizes of anatase and rutile crystallites calculated using Scherrer's equation can be found in the Supporting Information (Fig. S3).

Even the smallest amounts of iron(III) promote crystallization of anatase (Fig. 3, series calcined at 450°C) and inhibit antase to rutile

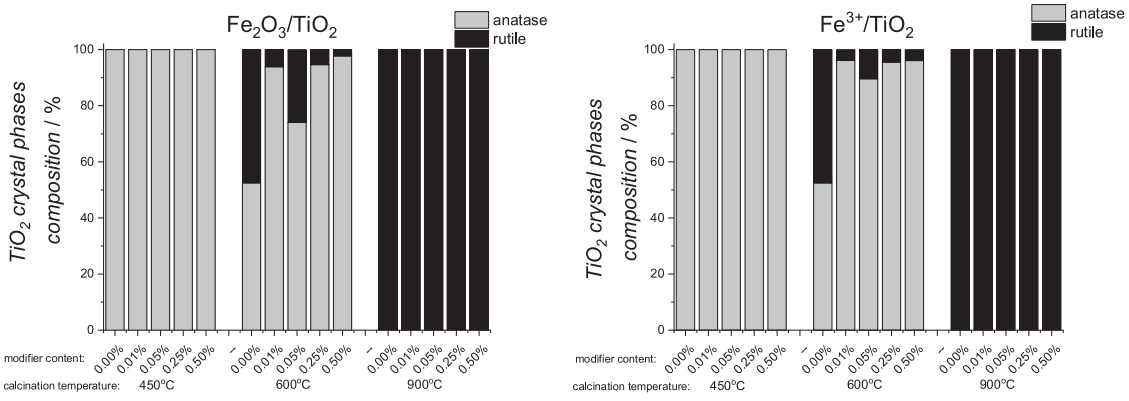

Fig. 3. Content of anatase and rutile in the prepared materials.

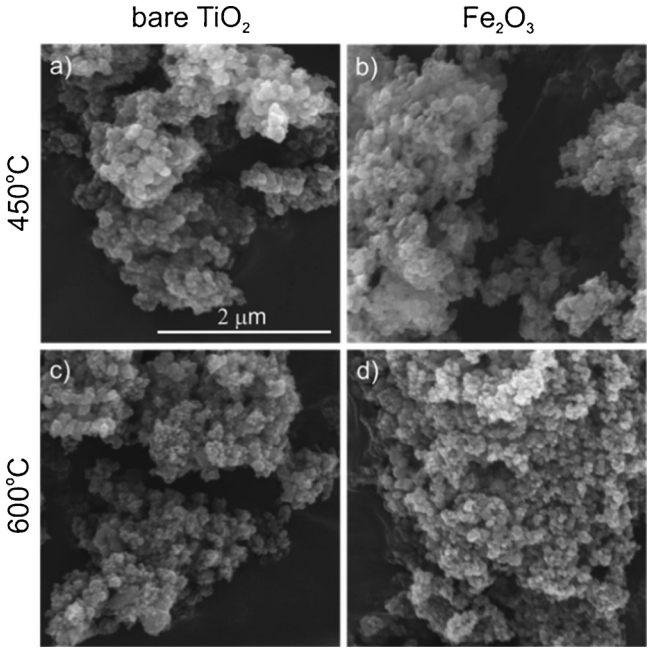

Fig. 4. SEM images of the materials calcined at 450°C (a, b) and 600°C (c, d). Left and right columns present bare TiO_2 (a, c) and TiO_2 modified with 0.01% mol Fe_2O_3 (b, d), respectively.

transformation (Fig. 3, series calcined at 600°C). However, there is no clear relationship between the concentration of Fe^{3+} or Fe_2O_3 and the phase composition. Introduction of iron(III) species does not influence significantly the size of anatase crystallites (compare SI). This observations are consistent with previously reported effect of the interstitial stabilisation of the titania lattice and consequent inhibition of antase to rutile transformation by iron (both ions and oxides) species [37,53–55].

SEM images of the studied materials (Fig. 4) show aggregates of TiO_2 crystallites. Addition of the modifier results in the enrichment of surface texture, which translates to the increased specific surface area (Fig. 5). Each studied concentration of the modifier enhances significantly the specific surface area and pore volumes of the materials. These parameters remain almost constant regardless of the modifier concentration within the 0.01-0.50%mol Fe:Ti range.

Spectral properties of the photocatalysts were studied using UV–vis DRS. In all sets of materials with the same concentration of Fe^{III} a bathochromic shift of the absorption edge with increasing calcination temperature can be observed (Fig. 6a). The materials calcined at 450,

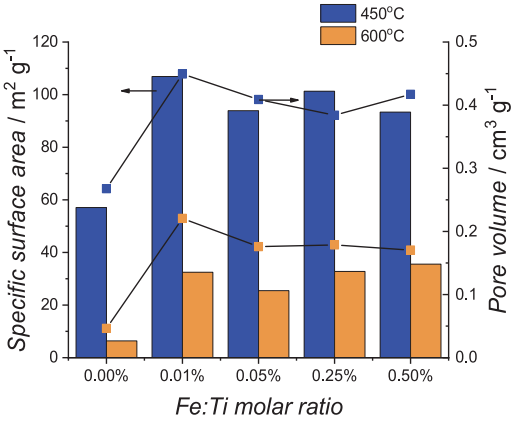

Fig. 5. Specific surface areas (bars) and pore volumes (squares) measured for the samples calcined at 450 and 600°C modified with iron(III) oxide.

600 and 900°C show characteristic spectra for anatase ($E_g \approx 3.2$ eV), anatase-rutile and rutile ($E_g \approx 3.0$ eV) phases, respectively (Fig. 3), which is consistent with XRD data.

The DRS analysis revealed that the addition of Fe^{III} species increases absorbance of the studied samples in visible light (Fig. 6b). Basing on the photocurrent measurements it can be concluded that this increase does not translate to the photosensitization (no photocurrents induced by visible light have been recorded, Fig. 7). The photoelectrochemical measurements showed also significant differences in photon to current conversion efficiency between bare TiO_2, Fe_2O_3/TiO_2 and Fe^{3+}/TiO_2. The highest photocurrents were recorded for the series of materials calcined at 600°C (other data not shown). Fe_2O_3/TiO_2 composite appears to be the most photoactive one, which is indicated by the most efficient interfacial electron transfer taking place at this electrode. These observations correlate well with the photocatalytic activity (*vide infra*).

EPR measurements revealed some significant information on the surrounding of the iron(III) species in the studied photocatalysts. In the case of the Fe^{3+} modifier, iron ions are incorporated into TiO_2 crystals already at 450°C (Fig. 8a). The signal at $g = 1.998$ marked with a single asterisk consists of at least two lines which are assigned to Fe^{III} ($S = 5/2$) built in the anatase lattice [56,57]. The sharp line originates from isolated octahedral Fe^{III} cations surrounded by Ti^{IV}, whereas a broad line is usually assigned to small iron oxide-type clusters wrapped up by the anatase matrix [58]. Incorporated iron only slightly enhances photocurrents and photocatalytic activity. Signals at $g = 4.3$, denoted with a double asterisk, correspond to Fe^{III}, presumably located at the surface of the particles in strongly distorted rhombic sites [56].

In the case of Fe_2O_3/TiO_2, iron does not incorporate into titania neither at 450 nor at 600°C. Fe incorporation into the TiO_2 matrix occurs when 900°C is reached (Fig. 8b) and is associated with the phase transition of anatase into rutile. In the both cases (Fe^{3+} and Fe_2O_3 modifications) sample calcination at this temperature leads to vanishing of previously described EPR signals and an appearance of several new peaks at $g_1 = 8.11$, $g_2 = 5.57$, $g_3 = 3.36$, $g_4 = 2.63$, $g_5 = 1.52$. The lines have been assigned to Fe^{III} ions substituting Ti^{IV} in the rutile lattice and revealing tetragonal sites of a distorted axial symmetry [59–61]. In the case of Fe_2O_3/TiO_2, the diffusion of iron ions is not observed at lower temperatures, whereas in the case of Fe^{3+} ions the process seems to proceed gradually with an increasing temperature.

3.2. Photocatalytic activity of iron(III)-modified materials

Generally, materials modified with iron(III) oxide were more photoactive in the process of Azure B degradation in comparison to the materials modified with iron(III) ions (Fig. 9). The P25 material has been used as a benchmark for photocatalytic activity tests. Apparently, photoactivity of both types of materials depends on the presence of iron. In the case of iron(III) oxide composites, the most active material contained 0.01%mol of iron (600°C). Although activity of iron(III) oxide in photodegradation of dyes (including the photo-Fenton reactivity) was reported [27,62], there is no clear correlation between Fe_2O_3 concentration and the Fe_2O_3/TiO_2 activity (Figs. 9, S5). In the case of the material containing 0.05%mol of Fe, even lower photoactivity has been observed, compared to bare TiO_2.

The addition of iron(III) species increased the photoactivity of the studied materials calcined at 450 and 600°C compared to unmodified ones (Fig. 10). The most active materials in TA hydroxylation were those with the smallest admixtures of iron(III) species (0.01%mol) calcined at 600°C. Materials calcined at 900°C showed a negligible activity.

The relationship between the photoactivity and Fe concentration was similar to that observed in the case of Azure B photodegradation. Such correlation could be expected, because the mentioned dye degradation is largely mediated by hydroxyl radicals. Nevertheless, other degradation pathways of AB leading to its complete mineralization

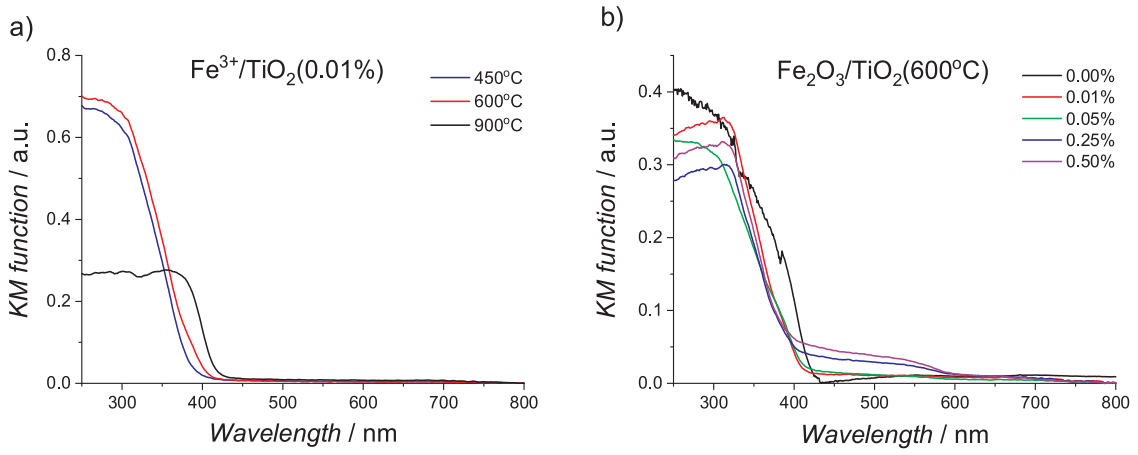

Fig. 6. Absorption spectra of series of materials synthesized in the presence of Fe^{3+} (a) and Fe_2O_3 (b).

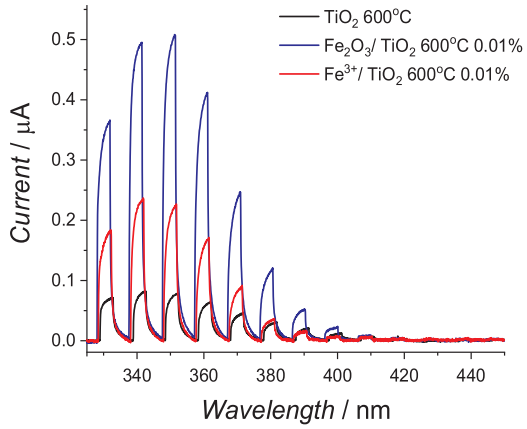

Fig. 7. Photocurrent generation at electrodes made of the studied materials recorded at 1 V *vs.* Ag/AgCl in deoxygenated 0.1 M KNO_3. All electrodes are characterized by a similar absorbance under UV light.

could also be involved, *e.g.*, oxidation with holes or reactions with other reactive oxygen species [63–66]. In the series of Fe^{3+}/TiO_2 materials some exceptions can be observed. The material with 0.01%mol of Fe^{3+} calcined at 600°C exhibited a similar activity to that of Fe_2O_3/TiO_2(600°C). However, with an increasing Fe^{3+} concentration the activity decreased remarkably, even below that of non-modified TiO_2. Noteworthy, under these conditions iron ions might be built in the crystal lattice of titanium dioxide, what is not the case for Fe_2O_3 materials (as confirmed by the EPR studies). This incorporation seems to be responsible for the deterioration of the material activity, what can be confirmed by a total inhibition of $HO^{\bullet}$ formation for all iron-containing materials calcined at 900°C. Noteworthy, in the case of 0.01%mol Fe^{3+}/TiO_2 materials, the photocatalytic activity (oxidation of terephthalic acid) was much higher for photocatalysts calcined at 600°C compared to those annealed at 450°C. Preeminence of 0.01%mol Fe^{3+}/TiO_2(600°C) resulted probably from its phase composition (anatase:rutile ratio) (Fig. 3). A significant synergistic effect observed when rutile and anatase are used simultaneously, which results in a higher photoactivity than that of each polymorph used separately, has been well documented [67–70]. The increasing content of Fe^{3+} diminishes the photoactivity of TiO_2.

The enhancement of the photocatalytic activity of modified materials does not appear as a direct consequence of the iron admixtures. At the lowest Fe_2O_3 concentrations this oxide could be expected to play a negligible role in the photocatalytic activity of the composite. At higher concentrations (materials containing 0.25%mol and 0.50%mol of Fe) a catalytic or photocatalytic nature of Fe_2O_3 may become more

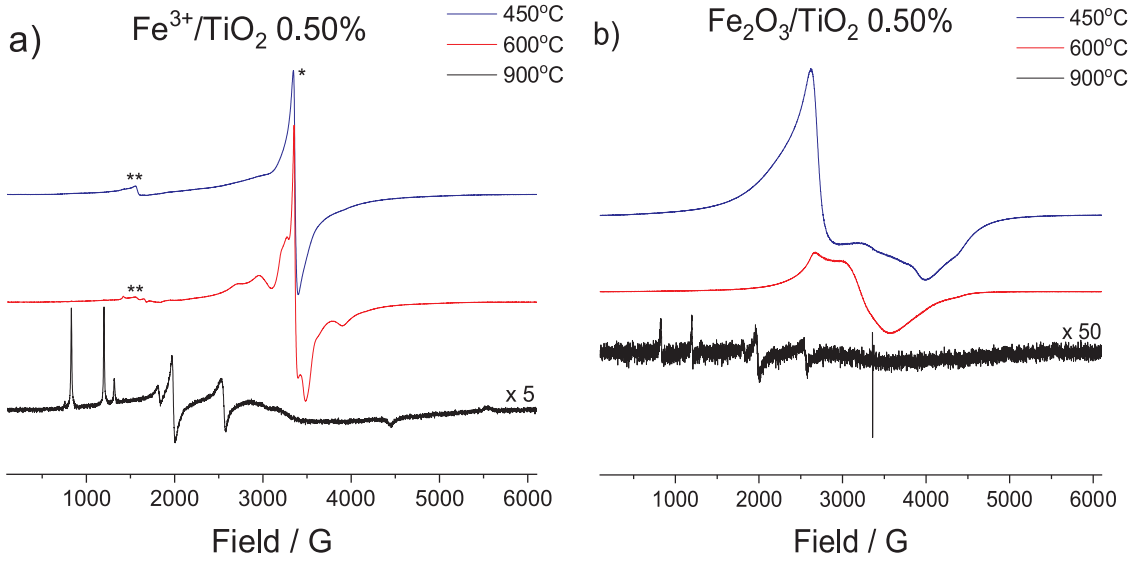

Fig. 8. EPR spectra of samples (0.50% of the modifier) recorded at room temperature: Fe^{3+}/TiO_2 (a); Fe_2O_3/TiO_2 (b). Spectra of materials calcined at 900°C were multiplied by the indicated factors.

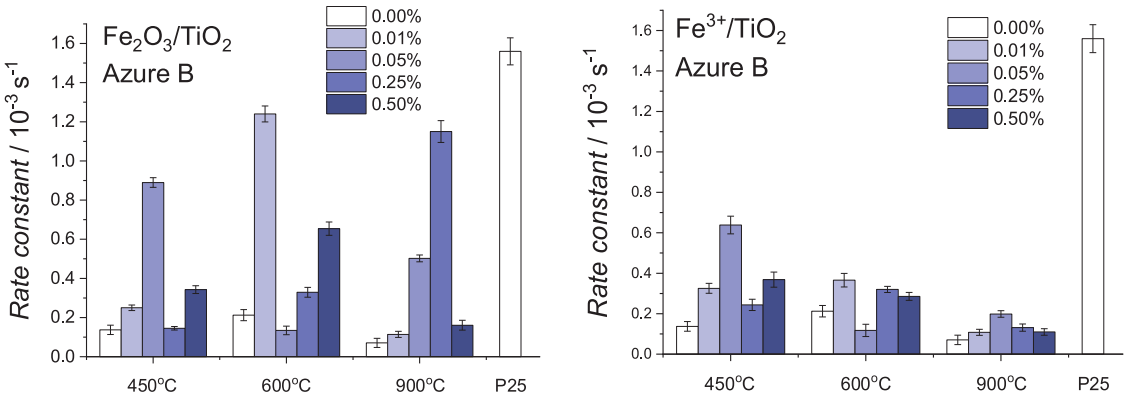

Fig. 9. Rate constants of the first order degradation process of Azure B in the presence of the studied materials.

pronounced, however, the observed photoactivity of materials did not confirm this expectations. On the other hand, XRD studies revealed that iron species influence the phase composition of the formed TiO_2. The higher photocatalytic activity and greater photocurrent generation efficiency may indicate a more effective interfacial electron transfer, better charge separation and, therefore, less efficient recombination of holes and electrons. All these effects may originate from a beneficial phase composition (anatase:rutile ratio). The observed high photocurrents and high photocatalytic activity of Fe_2O_3/TiO_2 composites and Fe^{3+}/TiO_2 materials calcined at 600°C can result from an altered phase transformation process. Therefore, iron(III) species, both Fe^{3+} ions and Fe_2O_3, can be considered as *phase-composition controllers* (PCC) for crystallization of TiO_2. Among all considered mechanisms involving the used modifiers the aforementioned effect seems to play a predominant role in increasing the photocatalytic activity of these materials.

To verify if this effect is specific only for iron(III) species or is a more general phenomenon, a set of TiO_2 materials modified with other metal species was prepared. Titania was modified with oxides and salts of cobalt(II), gallium, bismuth, tungsten(VI), molybdenum(VI), vanadium(V) and nickel(II). Determined phase compositions based on XRD data are presented in SI, Fig. S4. As anticipated, the data clearly shows that addition of any modifier influences the anatase to rutile ratio, similarly to the observation described for Fe^{3+} and Fe_2O_3. In a few cases (Mo and V species) modifiers in low concentration promoted rutile formation.

The DRS analysis revealed that the addition of metal species caused usually slight changes of light absorption (Fig. S8). The only exceptions were the photocatalyst modified with bismuth and vanadium species. Similarly to Fe/TiO_2 samples, materials calcined at 450, 600 and 900°C showed absorption spectra characteristic for anatase ($E_g \approx 3.2$ eV), anatase-rutile and rutile ($E_g \approx 3.0$ eV) phases.

For each material calcined at 600°C a decimal logarithm of anatase to rutile ratio, log(A/R), was calculated. The size of crystallites (Fig. 11), AB degradation rate and $HO^{\bullet}$ radical generation efficiency (in terms of TA oxidation; Fig. 12) were plotted against log(A/R) to check possible correlations.

The size distribution of anatase and rutile crystallites (Fig. 11) seems to depend neither on type of modification (oxide or ion), nor on amount of added modifier (0.01-0.50%mol). The size of anatase crystallites varies from 23 to 77 nm, whereas that of rutile from 75 to 372 nm. Apparently, during calcination at 600°C anatase crystals grow and eventually recrystallize to rutile. Therefore, the lower the content of anatase in the material, the larger the crystals. On the other hand, in the case of rutile, a similar correlation can be observed only for modifications with metal salts.

Apart from a few exceptions, it can be noticed that photocatalytic performance of prepared powders in the reaction of hydroxyl radicals generation strongly depends on anatase to rutile ratio, especially for TiO_2 materials modified with various metal oxides (Fig. 12). This can be concluded basing on the correlation coefficients, which for AB degradation are described as moderate/strong ($r = 0.67$) and for TA oxidation are high ($r = 0.73$) and very high ($r = 0.91$) for ions and oxides, respectively [71]. This leads to the conclusion that the actual phase composition of TiO_2 is more crucial than the crystal size, type or amount of the modifier, when its content is small (0.01 or 0.05%mol). Evidently, these small admixtures significantly alter anatase to rutile ratio and, therefore, this effect cannot be neglected. With this data, we can confirm our aforementioned hypothesis concerning the PCC role of admixed metal ions and oxides, apparently not limited to iron species. The modifiers are responsible for the enhanced photoactivity of the studied materials through their influence on the TiO_2 phase composition rather than their catalytic, photocatalytic, redox, spectral and other properties.

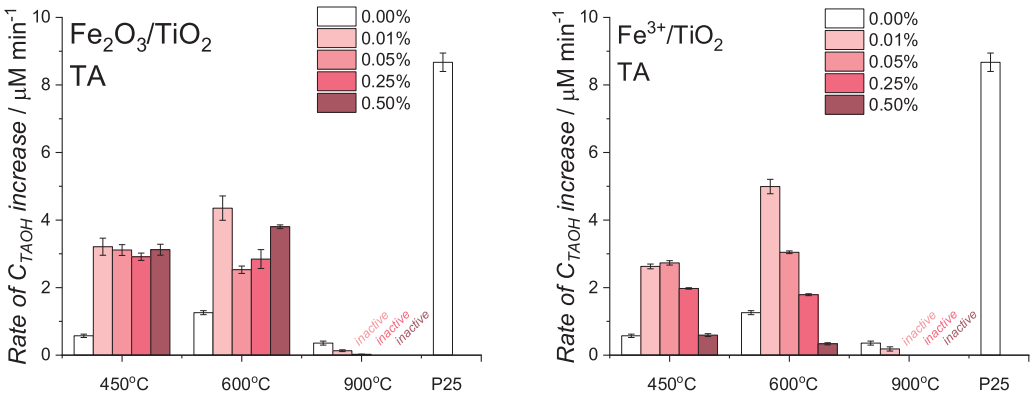

Fig. 10. The rates of hydroxyterephthalic acid formation in the presence of the studied photocatalysts.

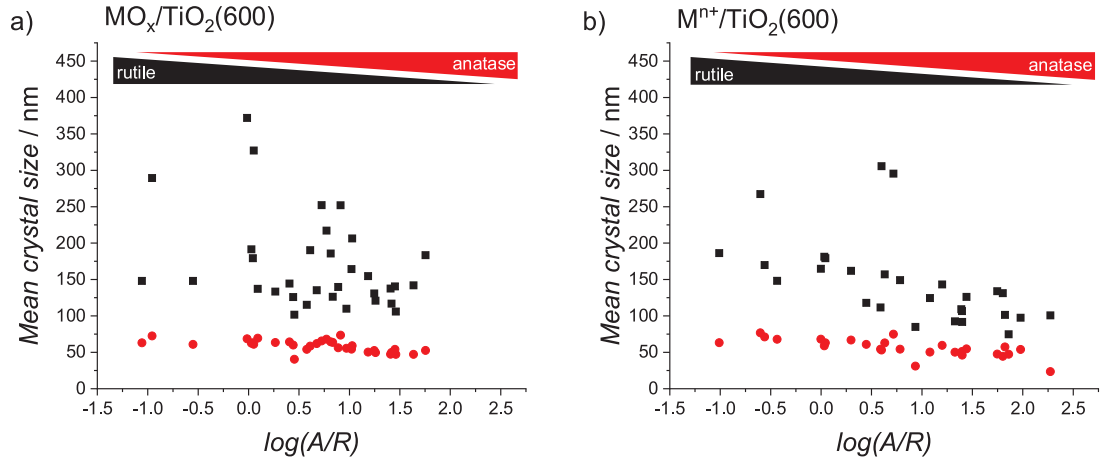

Fig. 11. Dependence of the mean anatase (circles) and rutile (squares) crystal size on anatase to rutile ratio (presented as a decimal logarithm) for TiO_2 materials modified with 0.01, 0.05, 0.25 and 0.50%mol of various metal oxides (a) and salts (b) calcined at 600°C. The triangles show schematically the relative amounts of TiO_2 phases.

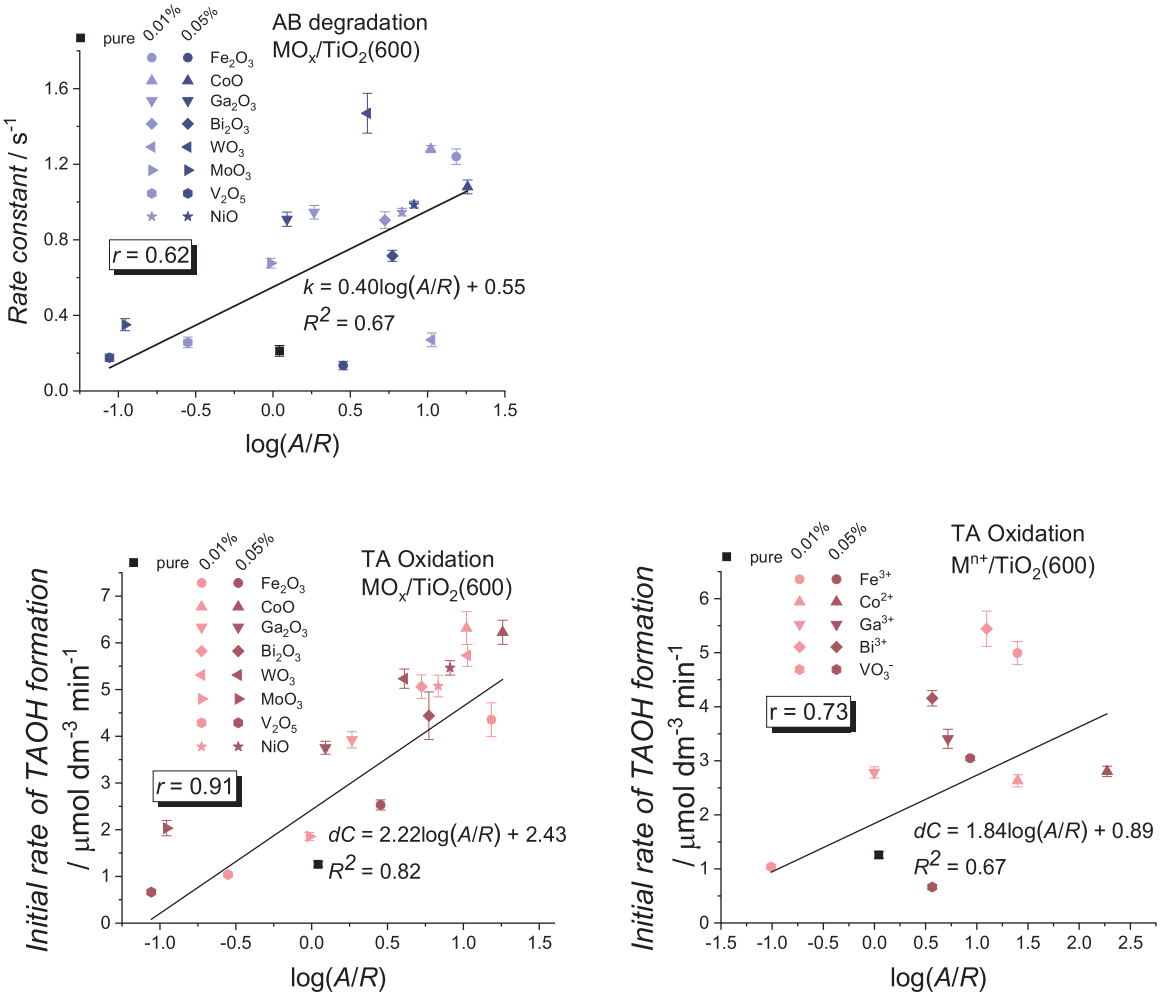

Fig. 12. Dependence of the rate constant of AB degradation and rates of TAOH formation on anatase to rutile ratio (presented as a decimal logarithm) for TiO_2 materials modified with 0.01 and 0.05%mol of various metal oxides and salts calcined at 600°C. Correlation coefficients (*r*), calculated with assumption of 5% level of significance, are shown in the frames.

4. Conclusions

Modification of titania with iron(III), as well as with most of other investigated metal compounds, clearly alters the properties of the photocatalysts. It favours the crystallization of anatase and inhibits its conversion to rutile. Also, the specific surface area and pore volumes are higher in the case of modified materials compared to the non-modified ones calcined at the same temperatures. These effects can be assigned to modifiers acting as PCC in the process of TiO_2 crystallization.

Materials modified with iron(III) oxide showed a higher activity in AB and TA photocatalytic oxidation. This leads to the conclusion that the composite materials (Fe_2O_3/TiO_2 calcined at 450 and 600°C) are more efficient compared to the doped ones (Fe^{3+}/TiO_2). It is worth noting, that the materials modified with Fe_2O_3 and calcined at 900°C should be considered as doped, because of incorporation of iron species into the lattice of TiO_2. This is consistent with the lower photoactivity of the doped materials.

Despite the observed absorption of visible light by the materials, no photosensitization occurs. This indicates that the improvement of the photocatalytic activity of the modified materials cannot be assigned to the presence of iron(III) species themselves, but rather to an indirect impact of Fe_2O_3 and Fe^{3+} on the properties of titanium dioxide. Broadening of this analysis to different metal species showed that this is a general feature of bulk modified TiO_2 synthesized by the sol-gel method. The parameter that seems to have a dominant influence on the resulting photoactivity is the anatase to rutile ratio. The higher the ratio, the better the photocatalytic performance of the materials. This observation was characterized with logarithmic dependence with good correlation coefficients.

This work shows that the role of modifiers on photocatalytic activity of TiO_2 materials must be carefully interpreted (and in several cases revisited). The modifiers, especially added in small amounts, may not be the direct source of changes of photocatalytic or catalytic behaviour of titania, but they can influence the structure and morphology of TiO_2. This role of modifiers may appear predominant and should never be neglected.

Acknowledgements

The studies were carried out thanks to the Polish National Science Centre (NCN) within the project no. 2014/15/N/ST4/03043. MT and MK are grateful for the support of NCN within the project no. 2015/19/B/ST5/00950.

Appendix A. Supplementary data

Supplementary material related to this article can be found, in the online version, at doi:https://doi.org/10.1016/j.apcatb.2019.01.074.

References

[1] S.J.A. Moniz, S.A. Shevlin, X. An, Z.X. Guo, J. Tang, Fe_2O_3–TiO_2 nanocomposites for enhanced charge separation and photocatalytic activity, Chem. Eur. J. 20 (2014) 15571–15579.
[2] Z. Shayegan, C.-S. Lee, F. Haghighat, TiO_2 photocatalyst for removal of volatile organic compounds in gas phase–a review, Chem. Eng. J. 334 (2018) 2408–2439.
[3] A. Mayoufi, M.F. Nsib, A. Houas, Doping level effect on visible-light irradiation W-doped TiO_2–anatase photocatalysts for Congo red photodegradation, C. R. Chim. 17 (2014) 818–823.
[4] T. Zhang, B. Yu, D. Wang, F. Zhou, Molybdenum-doped and anatase/rutile mixed-phase TiO_2 nanotube photoelectrode for high photoelectrochemical performance, J. Power Sources 281 (2015) 411–416.
[5] T.-D. Pham, B.-K. Lee, Novel adsorption and photocatalytic oxidation for removal of gaseous toluene by V-doped TiO_2/PU under visible light, J. Hazard. Mater. 300 (2015) 493–503.
[6] M. Nolan, Electronic coupling in iron oxide-modified TiO_2 leads to a reduced band gap and charge separation for visible light active photocatalysis, Phys. Chem. Chem. Phys. 13 (2011) 18194–18199.
[7] H. Tada, Q. Jin, A. Iwaszuk, M. Nolan, Molecular-scale transition metal oxide nanocluster surface-modified titanium dioxide as solar-activated environmental catalysts, J. Phys. Chem. C 118 (2014) 12077–12086.
[8] R. Daghrir, P. Drogui, D. Robert, Modified TiO_2 for environmental photocatalytic applications: a review, Ind. Eng. Chem. Res. 52 (2013) 3581–3599.
[9] M. Pelaez, N.T. Nolan, S.C. Pillai, M.K. Seery, P. Falaras, A.G. Kontos, P.S. Dunlop, J.W. Hamilton, J.A. Byrne, K. O'shea, A review on the visible light active titanium dioxide photocatalysts for environmental applications, Appl. Catal. B: Environ. 125 (2012) 331–349.
[10] C. Chen, X. Li, W. Ma, J. Zhao, H. Hidaka, N. Serpone, Effect of transition metal ions on the TiO_2-assisted photodegradation of dyes under visible irradiation: a probe for the interfacial electron transfer process and reaction mechanism, J. Phys. Chem. B 106 (2002) 318–324.
[11] P.D. Tran, L. Xi, S.K. Batabyal, L.H. Wong, J. Barber, J.S.C. Loo, Enhancing the photocatalytic efficiency of TiO_2 nanopowders for H_2 production by using non-noble transition metal co-catalysts, Phys. Chem. Chem. Phys. 14 (2012) 11596–11599.
[12] M.M. Momeni, Y. Ghayeb, Preparation of cobalt coated TiO_2 and WO_3–TiO_2 nanotube films via photo-assisted deposition with enhanced photocatalytic activity under visible light illumination, Ceram. Int. 42 (2016) 7014–7022.
[13] M. Abdullah, F.K. Chong, Preparation and characterization of tungsten-loaded titanium dioxide photocatalyst for enhanced dye degradation, J. Hazard. Mater. 176 (2010) 451–458.
[14] M.A. Abdullah, F.K. Chong, Dual-effects of adsorption and photodegradation of methylene blue by tungsten-loaded titanium dioxide, Chem. Eng. J. 158 (2010) 418–425.
[15] J.C.-S. Wu, C.-H. Chen, A visible-light response vanadium-doped titania nanocatalyst by sol–gel method, J. Photochem. Photobiol. A: Chem. 163 (2004) 509–515.
[16] B. Tryba, M. Piszcz, A.W. Morawski, Photocatalytic activity of TiO_2-WO_3 composites, Int. J. Photoenergy 2009 (2009).
[17] T.S. Natarajan, K. Natarajan, H.C. Bajaj, R.J. Tayade, Enhanced photocatalytic activity of bismuth-doped TiO_2 nanotubes under direct sunlight irradiation for degradation of Rhodamine B dye, J. Nanopart. Res. 15 (2013) 1669.
[18] C.C. Pei, W.W.-F. Leung, Photocatalytic oxidation of nitrogen monoxide and o-xylene by TiO_2/ZnO/Bi_2O_3 nanofibers: optimization, kinetic modeling and mechanisms, Appl. Catal. B: Environ. 174 (2015) 515–525.
[19] J.G. Mahy, L. Tasseroul, M. Herlitschke, R.P. Hermann, S.D. Lambert, Fe^{3+}/iron oxide/SiO_2 xerogel catalysts for p-nitrophenol degradation by photo-Fenton effects: influence of thermal treatment on catalysts texture, Mater. Today 3 (2016) 464–469.
[20] S.A.K. Leghari, S. Sajjad, F. Chen, J. Zhang, WO_3/TiO_2 composite with morphology change via hydrothermal template-free route as an efficient visible light photocatalyst, Chem. Eng. J. 166 (2011) 906–915.
[21] T. Amna, M.S. Hassan, M. Pandurangan, M.-S. Khil, H.-K. Lee, I. Hwang, Characterization and potent bactericidal effect of cobalt doped titanium dioxide nanofibers, Ceram. Int. 39 (2013) 3189–3193.
[22] M. Faisal, F.A. Harraz, A.A. Ismail, A.M. El-Toni, S. Al-Sayari, A. Al-Hajry, M. Al-Assiri, Novel mesoporous NiO/TiO_2 nanocomposites with enhanced photocatalytic activity under visible light illumination, Ceram. Int. 44 (2018) 7047–7056.
[23] K. Szaciłowski, W. Macyk, A. Drzewiecka-Matuszek, M. Brindell, G. Stochel, Bioinorganic photochemistry: frontiers and mechanisms, Chem. Rev. 105 (2005) 2647–2694.
[24] J. Richard, Characterisation of iron/titanium oxide photocatalysts. Part 1.—structural and magnetic studies, J. Chem. Soc. Faraday Trans. 88 (1992) 377–383.
[25] R.I. Bickley, T. Gonzalez-Carreno, A.R. Gonzalez-Elipe, G. Munuera, L. Palmisano, Characterisation of iron/titanium oxide photocatalysts. Part 2.—surface studies, J. Chem. Soc. Faraday Trans. 90 (1994) 2257–2264.
[26] M. Liu, X. Qiu, M. Miyauchi, K. Hashimoto, Energy-level matching of Fe(III) ions grafted at surface and doped in bulk for efficient visible-light photocatalysts, J. Am. Chem. Soc. 135 (2013) 10064–10072.
[27] Y. Liu, H. Yu, S. Zhan, Y. Li, Z. Lv, X. Yang, Y. Yu, Fast degradation of methylene blue with electrospun hierarchical α-Fe_2O_3 nanostructured fibers, J. Solgel Sci. Technol. 58 (2011) 716–723.
[28] S. Sood, A. Umar, S.K. Mehta, S.K. Kansal, Highly effective Fe-doped TiO_2 nanoparticles photocatalysts for visible-light driven photocatalytic degradation of toxic organic compounds, J. Colloid Interface Sci. 450 (2015) 213–223.
[29] A.S. Ganeshraja, K. Rajkumar, K. Zhu, X. Li, S. Thirumurugan, W. Xu, J. Zhang, M. Yang, K. Anbalagan, J. Wang, Facile synthesis of iron oxide coupled and doped titania nanocomposites: tuning of Physicochemical and photocatalytic properties, RSC Adv. 6 (2016) 72791–72802.
[30] B. Palanisamy, C. Babu, B. Sundaravel, S. Anandan, V. Murugesan, Sol–gel synthesis of mesoporous mixed Fe_2O_3/TiO_2 photocatalyst: application for degradation of 4-chlorophenol, J. Hazard. Mater. 252 (2013) 233–242.
[31] O. Avilés-García, J. Espino-Valencia, R. Romero, J.L. Rico-Cerda, M. Arroyo-Albiter, R. Natividad, W and Mo doped TiO_2: synthesis, characterization and photocatalytic activity, Fuel 198 (2017) 31–41.
[32] A. Mayoufi, M.F. Nsib, A. Houas, Doping level effect on visible-light irradiation W-doped TiO_2–anatase photocatalysts for Congo red photodegradation, C. R. Chim. 17 (2014) 818–823.
[33] L. Mahoney, R. Peng, C.-M. Wu, J. Baltrusaitis, R.T. Koodali, Solar simulated hydrogen evolution using cobalt oxide nanoclusters deposited on titanium dioxide mesoporous materials prepared by evaporation induced self-assembly process, Int. J. Hydrogen Energy 40 (2015) 10795–10806.
[34] Y. Wang, C.S. Liu, F.B. Li, C.P. Liu, J.B. Liang, Photodegradation of polycyclic aromatic hydrocarbon pyrene by Iron oxide in solid phase, J. Hazard. Mater. 162 (2009) 716–723.
[35] H. Tang, D. Zhang, G.G. Tang, X.R. Ji, W.J. Li, C.S. Li, X.F. Yang, Hydrothermal synthesis and visible-light photocatalytic activity of α-Fe_2O_3/TiO_2 composite hollow microspheres, Ceram. Int. 39 (2013) 8633–8640.
[36] O. Akhavan, Thickness Dependent Activity of Nanostructured TiO_2/α-Fe_2O_3 Photocatalyst Thin Films, Appl. Surf. Sci. 257 (2010) 1724–1728.
[37] D.A.H. Hanaor, C.C. Sorrell, Review of the anatase to rutile phase transformation, J. Mater. Sci. 46 (2011) 855–874.
[38] Z. Wei, E. Kowalska, B. Ohtani, Influence of post-treatment operations on structural properties and photocatalytic activity of octahedral anatase titania particles prepared by an ultrasonication-hydrothermal reaction, Molecules 19 (2014) 19573–19587.
[39] L. Samet, J.B. Nasseur, R. Chtourou, K. March, O. Stephan, Heat treatment effect on the physical properties of cobalt doped TiO_2 sol–gel materials, Mater. Charact. 85 (2013) 1–12.

[40] E.O. Oseghe, P.G. Ndungu, S.B. Jonnalagadda, Photocatalytic degradation of 4-chloro-2-methylphenoxyacetic acid using W-doped TiO_2, J. Photochem. Photobiol. A: Chem. 312 (2015) 96–106.
[41] E.P. Melián, M.N. Suárez, T. Jardiel, J.M.D. Rodríguez, A.C. Caballero, J. Araña, D.G. Calatayud, O.G. Díaz, Influence of nickel in the hydrogen production activity of TiO_2, Appl. Catal. B: Environ. 152 (2014) 192–201.
[42] J. Ding, Q. Zhong, H. Gu, Iron-titanium dioxide composite nanoparticles prepared with an energy effective method for efficient visible-light-driven photocatalytic nitrogen reduction to ammonia, J. Alloys Compd. 746 (2018) 147–152.
[43] J. Ma, H. He, F. Liu, Effect of Fe on the photocatalytic removal of NO_x over visible light responsive Fe/TiO_2 catalysts, Appl. Catal. B: Environ. 179 (2015) 21–28.
[44] S.N.R. Inturi, T. Boningari, M. Suidan, P.G. Smirniotis, Visible-light-induced photodegradation of gas phase acetonitrile using aerosol-made transition metal (V, Cr, Fe, Co, Mn, Mo, Ni, Cu, Y, Ce, and Zr) doped TiO_2, Appl. Catal. B: Environ. 144 (2014) 333–342.
[45] P. Jiang, W. Xiang, J. Kuang, W. Liu, W. Cao, Effect of cobalt doping on the electronic, optical and photocatalytic properties of TiO_2, Solid State Sci. 46 (2015) 27–32.
[46] H. Tada, Q. Jin, H. Nishijima, H. Yamamoto, M. Fujishima, Si. Okuoka, T. Hattori, Y. Sumida, H. Kobayashi, Titanium(IV) dioxide surface-modified with iron oxide as a visible light photocatalyst, Angew. Chem. Int. Ed. 50 (2011) 3501–3505.
[47] W. Macyk, A. Franke, G. Stochel, Metal compounds and small molecules activation–case studies, Coord. Chem. Rev. 249 (2005) 2437–2457.
[48] S.G. Kumar, K.K. Rao, Comparison of modification strategies towards enhanced charge carrier separation and photocatalytic degradation activity of metal oxide semiconductors (TiO_2, WO_3 and ZnO), Appl. Surf. Sci. 391 (2017) 124–148.
[49] P. Bansal, A. Verma, Novel Fe-TiO_2 composite driven dual effect for reduction in treatment time of pentoxifylline: slurry to immobilized approach, Mater. Des. 125 (2017) 135–145.
[50] Y. Liu, W. Jin, Y. Zhao, G. Zhang, W. Zhang, Enhanced catalytic degradation of methylene blue by α-Fe_2O_3/graphene oxide via heterogeneous photo-Fenton reactions, Appl. Catal. B: Environ. 206 (2017) 642–652.
[51] A.A. Isari, A. Payan, M. Fattahi, S. Jorfi, B. Kakavandi, Photocatalytic degradation of rhodamine B and real textile wastewater using Fe-doped TiO_2anchored on reduced graphene oxide (Fe-TiO_2/rGO): Characterization and feasibility, mechanism and pathway studies, Appl. Surf. Sci. 462 (2018) 549–564.
[52] T. Hirakawa, Y. Nosaka, Properties of $O_2^{\bullet-}$ and $OH^{\bullet}$ formed in TiO_2 aqueous suspensions by photocatalytic reaction and the influence of H_2O_2 and some ions, Langmuir 18 (2002) 3247–3254.
[53] J.O. Carneiro, V. Teixeira, A. Portinha, A. Magalhaes, P. Coutinho, C.J. Tavares, R. Newton, Iron-doped photocatalytic TiO_2 sputtered coatings on plastics for self-cleaning applications, Mater. Sci. Eng. B 138 (2007) 144–150.
[54] Y. Iida, S. Ozaki, Grain growth and phase transformation of titanium oxide during calcination, J. Am. Ceram. Soc. 44 (1961) 120–127.
[55] K.J.D. MacKenzie, Calcination of titania: V, Kinetics and mechanism of the anatase-rutile transformation in the presence of additives, Trans. J. Br. Ceram. Soc. 74 (1975) 77–84.
[56] A. Amorelli, J.C. Evans, C.C. Rowlands, T.A. Egerton, An electron spin resonance study of rutile and anatase titanium dioxide polycrystalline powders treated with transition-metal ions, J. Chem. Soc. Faraday Trans. 1 83 (1987) 3541–3548.
[57] J. Soria, J.C. Conesa, V. Augugliaro, L. Palmisano, M. Schiavello, A. Sclafani, Dinitrogen photoreduction to ammonia over titanium dioxide powders doped with ferric ions, J. Phys. Chem. 95 (1991) 274–282.
[58] S. Yu, H.J. Yun, D.M. Lee, J. Yi, Preparation and characterization of Fe-doped TiO_2 nanoparticles as a support for a high performance CO oxidation catalyst, J. Mater. Chem. 22 (2012) 12629–12635.
[59] T.A. Egerton, E. Harris, E.J. Lawson, B. Mile, C.C. Rowlands, An EPR study of diffusion of Iron into rutile, Phys. Chem. Chem. Phys. 3 (2001) 497–504.
[60] A.I. Kokorin, R. Amal, W.Y. Teoh, A.I. Kulak, Studies of nanosized iron-doped TiO_2 photocatalysts by spectroscopic methods, Appl. Magn. Reson. (2017) 447–459.
[61] S. Neubert, D. Mitoraj, S.A. Shevlin, P. Pulisova, M. Heimann, Y. Du, G.K. Goh, M. Pacia, K. Kruczała, S. Turner, Highly efficient rutile TiO_2 photocatalysts with single Cu(II) and Fe(III) surface catalytic sites, J. Mater. Chem. A 4 (2016) 3127–3138.
[62] S. Kalal, N.P.S. Chauhan, N. Ameta, R. Ameta, S. Kumar, P.B. Punjabi, Role of copper pyrovanadate as heterogeneous photo-fenton like catalyst for the degradation of neutral red and Azure-B: an eco-friendly approach, Korean J. Chem. Eng. 12 (2014) 2183–2191.
[63] A. Houas, H. Lachheb, M. Ksibi, E. Elaloui, C. Guillard, J.-M. Herrmann, Photocatalytic degradation pathway of methylene blue in water, Appl. Catal. B: Environ. 31 (2001) 145–157.
[64] H. Gnaser, M.R. Savina, W.F. Calaway, C.E. Tripa, I.V. Veryovkin, M.J. Pellin, Photocatalytic degradation of methylene blue on nanocrystalline TiO_2: surface mass spectrometry of reaction intermediates, Int. J. Mass Spectrom. 245 (2005) 61–67.
[65] Y. Galagan, W.-F. Su, Reversible photoreduction of methylene blue in acrylate media containing benzyl dimethyl ketal, J. Photochem. Photobiol. A: Chem. 195 (2008) 378–383.
[66] A. Mills, J. Wang, Photobleaching of methylene blue sensitised by TiO_2: an ambiguous system? J. Photochem. Photobiol. A: Chem. 127 (1999) 123–134.
[67] S. Bakardjieva, J. Šubrt, V. Štengl, M.J. Dianez, M.J. Sayagues, Photoactivity of anatase–rutile TiO_2 nanocrystalline mixtures obtained by heat treatment of homogeneously precipitated anatase, Appl. Catal. B: Environ. 58 (2005) 193–202.
[68] R. Su, R. Bechstein, L. Sø, R.T. Vang, M. Sillassen, B. Esbjornsson, A. Palmqvist, F. Besenbacher, How the anatase-to-rutile ratio influences the photoreactivity of TiO_2, J. Phys. Chem. C 115 (2011) 24287–24292.
[69] R. Bacsa, J. Kiwi, Effect of rutile phase on the photocatalytic properties of nanocrystalline titania during the degradation of p-coumaric acid, Appl. Catal. B: Environ. 16 (1998) 19–29.
[70] M. Buchalska, M. Kobielusz, A. Matuszek, M. Pacia, S. Wojtyła, W. Macyk, On oxygen activation at rutile- and Anatase-TiO_2, ACS Catal. 5 (2015) 7424–7431.
[71] R. Taylor, Interpretation of the correlation coefficient: a basic review, J. Diagn. Med. Sonogr. 6 (1990) 35–39.